Chemical Engineering Journal 150 (2009) 55–62

Contents lists available at ScienceDirect

Chemical Engineering Journal

journal homepage: www.elsevier.com/locate/cej

Adsorption/desorption behavior of acid orange 10 on magnetic silica modified with amine groups

Asem A. Atia, Ahmed M. Donia*, Waheeba A. Al-Amrani

Chemistry Department, Faculty of Science, Menoufia University, Shebin El-Kom, Egypt

ARTICLE INFO

Article history:
Received 26 June 2008
Received in revised form 4 September 2008
Accepted 3 December 2008

Keywords:
Magnetic silica
Modified silica
Acid dyes
Adsorption
Water treatment

ABSTRACT

Two silica samples were prepared through precipitation of silica in the presence and absence of magnetite particles (Fe_3O_4). The products were immobilized with 3-aminopropyltriethoxysilane and characterized by means of FT-IR and X-ray. Surface area (BET), pore volume and pore diameter were also measured. The adsorption behavior of both silicas towards C.I. acid orange 10 in aqueous solutions was studied at different experimental conditions including contact time, pH and initial concentrations. The monoamine modified magnetic silica (MAMMS) displayed higher and faster adsorption relative to magnetite free one (MAMPS). The maximum adsorption capacity of the dye on MAMPS and MAMMS are 48.98 and 61.33 mg g^{-1}, respectively. Adsorption of the dye on both MAMMS and MAMPS fitted to Langmuir adsorption model and followed the pseudo-second order kinetics. The values of Gibbs free energy of adsorption (ΔG^0) were found to be −26.52 and −28.49 kJ/mol at 298 K for MAMPS and MAMMS, respectively. These negative values indicated the spontaneity of the adsorption of the dye on both silica samples. Regeneration of the dye-loaded silica was carried out using aqueous solution of pH 10. Desorption ratio of 98% was obtained over three adsorption/desorption cycles.

1. Introduction

Industrial development is pervasively connected to the disposal of a large number of various toxic pollutants including dyes. Dyes are present in the wastewater streams of many industrial sectors such as, dyeing, textile, tannery and the paint industry [1]. Dye bath effluents are not only aesthetic pollutants by their color but also interfere with light penetration that disturbs biological processes [2]. The total dye consumption of the textile industry worldwide is in excess of 10^7 kg per year. Consequently, one million kilograms per year of dyes are discharged into waste streams by the textile industry [3,4]. Many of conventional treatment technologies for dye removal have investigated extensively such as chemical coagulation or flocculation combined with flotation and filtration, membrane filtration, oxidation, and photo-degradation processes [5,6]. The adsorption process provides an attractive method for the treatment of textile effluent especially if the adsorbent is inexpensive and readily available [7,8]. The adsorption of acid dyes has been studied using different adsorbents; bentonite [5], hectorite [7], peat [9], activated bleaching earth [10], chitosan [11], montmorillonite [12], titania–silica composite [13], etc.

Among inorganic compounds, silica deserves particular attention, considering its stability, very low degree of swelling, controlled porosity and the chemical reactivity of their surfaces, resulting from the presence of silanol groups [14]. Coating magnetic particles with silica is becoming a promising and important approach in development of magnetic particles for both fundamental study and technology application [15]. Many of investigators used magnetic silica carriers for DNA purification and immobilization [16,17], protein adsorption [18], enzyme immobilization [19], etc. Little work has been found in the literature related to the use of magnetic silica in removal of dyes from their aqueous solutions.

Azo dyes are an interesting class of compounds that are widely used in textile industries [20]. In this study, precipitated and magnetic silica samples were prepared and immobilized with 3-aminopropyltriethoxysilane. The adsorption/desorption behavior of acid orange 10 (as a model of azo dyes) on the obtained silica samples was clarified. Kinetic and thermodynamic parameters of adsorption were calculated.

2. Materials and methods

2.1. Materials

3-Aminopropyltriethoxysilane (APTS) was purchased from Fluka, Italy; silica gel and C.I. acid orange 10 (AO-10) (80%) were obtained from Sigma–Aldrich Chemical Co., Germany. All other

* Corresponding author.
E-mail addresses: asemali2010@yahoo.com (A.A. Atia), ahmeddonia2003@yahoo.com (A.M. Donia), al_amrani2003@yahoo.com (W.A. Al-Amrani).

1385-8947/$ – see front matter © 2009 Elsevier B.V. All rights reserved.
doi:10.1016/j.cej.2008.12.004

chemicals were of analytical grade and were used as received. $FeSO_4{\cdot}7H_2O$ and $FeCl_3{\cdot}6H_2O$ were used as sources for Fe(II) and Fe(III), respectively.

2.2. Preparation of magnetite

Magnetite was prepared following the modified Massart method [21]. A 250 cm^3 of 0.2 mol dm^{-3} Fe(III) solution was added with stirring to a freshly prepared 250 cm^3 of 1.2 mol dm^{-3} Fe(II) solution. A 200 cm^3 of (30%) NH_4OH was suddenly poured to the previously prepared Fe(III)/Fe(II) solution while vigorous stirring was going on. A black precipitate was allowed to precipitate for 30 min with stirring. The precipitate was washed with deoxygenated water (water was boiled to repeal any gases then bubbled with nitrogen gas) under magnetic decantation until the acidity of suspension became below pH 7.5. The precipitate was dried at ambient temperature to give a black powder.

2.3. Preparation of magnetic silica

Five grams of silica was dissolved in 120 cm^3 of 4 mol dm^{-3} NaOH solution with heating to 353 K and stirring until completely dissolution. A half gram of grinded Fe_3O_4 was dispersed in 100 cm^3 of NaOH. The pH of the two solutions was adjusted to 12–13 by 2 mol dm^{-3} HCl. Sodium silicate solution was poured into the magnetite suspension with stirring for 30 min at 353 K. Hydrochloric acid of 2 mol dm^{-3} was added dropwise to adjust the pH value to 8 ± 0.2. The obtained precipitate was washed several times with bi-distilled water and then dispersed in 100 cm^3 of methanol. The silica-coated magnetite particles were removed from the medium using a magnet. The magnetite free precipitated silica was obtained following the same procedure in the absence of magnetite.

2.4. Immobilization of precipitated silicas with monoamine

Magnetite-coated silica and magnetite-free silica obtained in the above step were loaded by monoamine as follows: one cubic centimetre of 3-aminopropyltriethoxysilane (APTS) was dissolved in 100 cm^3 of bi-distilled water acidified with acetic acid (pH 4). Two grams of precipitated silicas (activated by drying in an oven at 423 K for 18 h) was added in the silane solution and stirred for 2 h at room temperature. The products were filtered off and kept in an oven at 393 K for 4 h. The dried products were washed repeatedly with distilled water, ethanol, and acetone to remove the unreacted material and then dried in the oven at 393 K for another 2 h and then referred as MAMMS (for magnetic-silica) and MAMPS (for magnetite-free silica) [22].

2.5. Characterization of the modified silicas

Nitrogen specific surface area (BET) of the obtained modified silicas was measured at 77.35 K by Quantachrome Instrument, NOVA 2000 series, USA using nitrogen as the sorbate. All measurements were taken after heating the samples up to 403 K and evacuation at a pressure of 10^{-4} Torr for 4 h. FT-IR measurements were performed in KBr discs using Nexeus-Nicolite-640-MSA FT-IR, Thermo Electronics Co., USA. X-ray diffraction (XRD) was carried out using Philips X-ray diffractometer model PW 1775 with Cu Kα radiation and Ni filter.

The chemical stability of the magnetite containing silica was checked by soaking silica-coated magnetite particles in strong acidic medium (pH 3) for 3 h. No appreciable dissolution of magnetite was observed. This indicates that the investigated silica displays a good chemical stability in strong acidic medium.

2.6. Preparation of AO-10 solutions and concentration measurements

Stock solution (240 mg dm^{-3}) of the investigated dye was prepared in bi-distilled water. The desired concentrations were obtained through dilution. The concentration of the dye was measured by spectrophotometric method [7]. Calibration curve of the investigated dye was prepared by measuring its absorbance against concentration at λ_{max} 475 nm using UV/vis spectrophotometer Model SP-850, Metertech Inc., Taipei, Taiwan, with 1.0 cm pathlength cell. Adsorption of the dye on the silica samples obtained was determined using the mass balance equation [4]:

$$q = \frac{(C_i - C_f) \times V}{W} \quad (1)$$

where q represents the amount of dye adsorbed (mg g^{-1}), C_i and C_f are the initial and final concentrations of dye (mg dm^{-3}), V is the volume of solution (dm^3) and W is the weight of silica sample (g).

3. Batch adsorption

3.1. Effect of pH

The effect of acidity of the medium on the adsorption of AO-10 on modified silicas was investigated at 298 K. Portions of 0.1 g of dry silica samples were placed in a series of flasks containing 20 cm^3 of stock solution of 240 mg dm^{-3} of dye. The desired pH was controlled by 2 mol dm^{-3} HCl and 2 mol dm^{-3} NaOH. The solution was completed to 100 cm^3 with bi-distilled water to give initial concentration of 48 mg dm^{-3} of dye. The contents of the flasks were equilibrated on a Gallenhamp Shaker, England, at 400 rpm for 4 h. The residual concentration of the dye in each flask was determined spectrophotometrically at λ_{max} 475 nm.

3.2. Effect of contact time

The effect of contact time on the adsorption was studied by placing 0.1 g samples of dry silica in a series of flasks each contains 20 cm^3 of stock solution of dye of concentration 240 mg dm^{-3} at pH 3 and 298 K. The solution was completed to 100 cm^3 with bi-distilled water to give initial concentration of 48 mg dm^{-3} of dye. The flasks were removed from the shaker at different time intervals. Five cubic centimeters of the solution was taken and centrifuged to determine the residual concentration of the dye as above.

3.3. Isotherms

Complete adsorption isotherms were obtained by placing samples of 0.1 g of dry silica in a series of flasks containing 100 cm^3 of dye solution at the desired initial concentrations (40–160 mg dm^{-3}) and at pH 3. The flasks were conditioned for 4 h at 400 rpm while keeping the temperature constant at 298, 313, 323 or 333 K. Later on, the residual concentration of the dye was estimated.

3.4. Desorption

Silica sample was loaded by the dye as follows: a 0.1 g of dry sample was added to a flask containing 20 cm^3 of stock solution of dye of concentration of 240 mg dm^{-3} at pH 3. The solution was completed to 100 cm^3 with bi-distilled water to give initial concentration of dye of 48 mg dm^{-3}. The flask was conditioned for 4 h at 400 rpm while keeping the temperature at 298 K. Later on, the contents of the flask were filtered off and the dye-loaded silica was placed in another flask containing 100 cm^3 of aqueous solution at pH 7–10 using 2 mol dm^{-3} NaOH. The flask was agitated at 400 rpm for 2 h at 298 K. The concentration of the dye released was estimated as

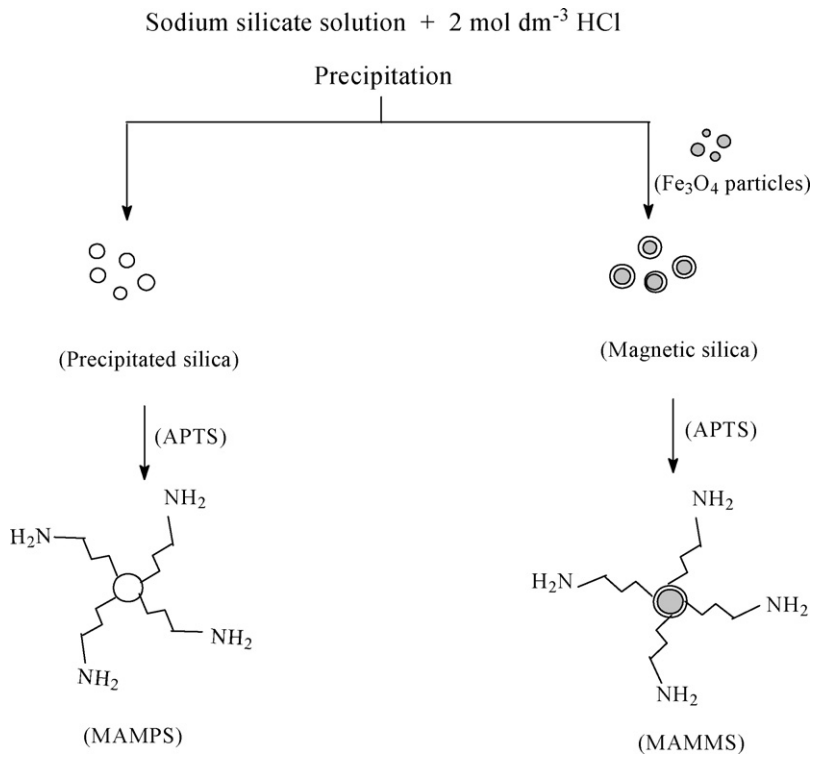

Fig. 1. Routs of preparation of MAMPS and MAMMS.

mentioned earlier. The ratio of desorption was calculated using the relation:

$$\text{Desorption}\,(\%) = \frac{\text{Total adsorption capacity after elution}}{\text{Total adsorption capacity before elution}} \times 100$$

4. Quantum chemical calculations

Geometry optimization of AO-10 molecules and its interaction with silica surface has been carried out using the semi-empirical AM1 methodology [23] as implemented in G98Wsuite of programs

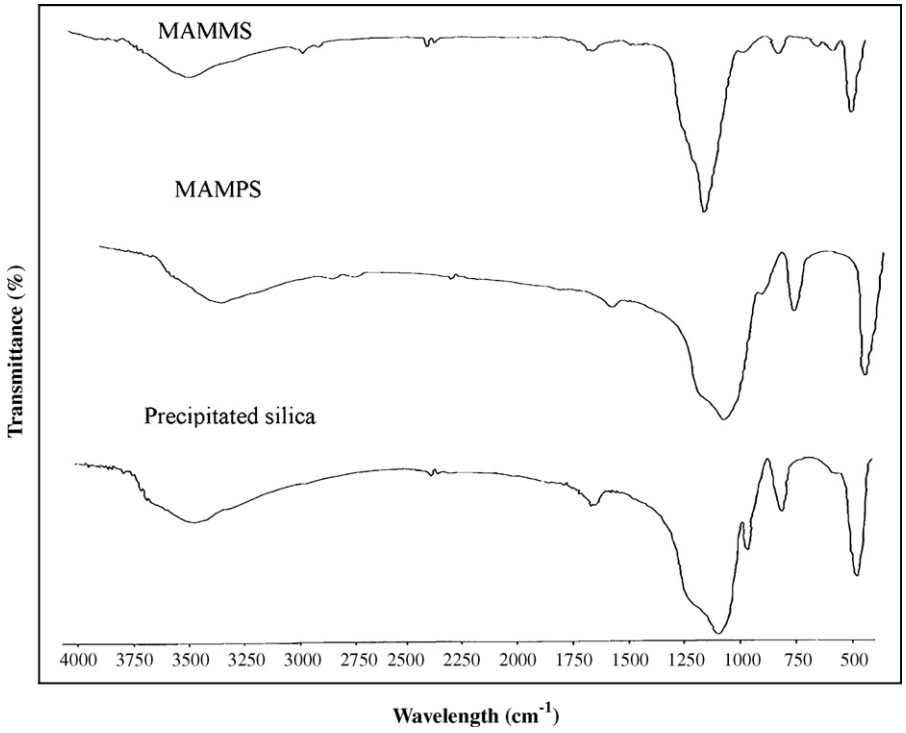

Fig. 2. FT-IR for precipitated silica, MAMPS and MAMMS.

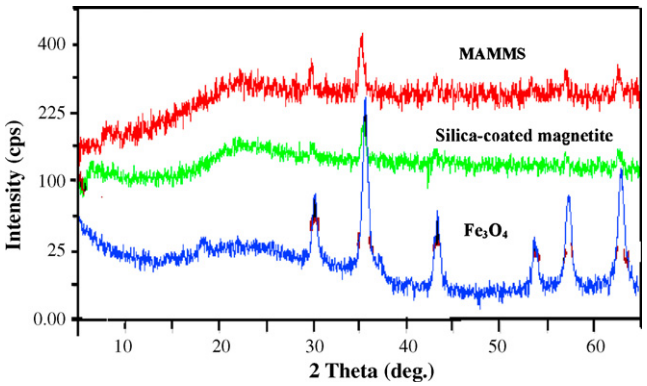

Fig. 3. XRD patterns for magnetite, silica-coated magnetite and MAMMS.

[24]. Frequency calculations have also been performed to ensure that the optimized structures represent minima of its respective potential energy surface.

5. Results and discussions

5.1. Characterization of modified silicas

The preparation of precipitated silicas was carried out according to the reaction routes shown in Fig. 1. FT-IR spectra of the precipitated and modified silica are shown in Fig. 2. FT-IR spectrum of the precipitated silica displayed a number of characteristic bands near 3446 cm^{-1} (broad), 1096 cm^{-1} (vs) and 799 (m) cm^{-1}. These bands are assigned to stretching vibration of H-bonded silanol group ν(≡Si—OH) along with physisorbed water ν(—OH), ν(≡Si—O—Si≡) of siloxane backbone, ν(≡Si—OH) of free silanol group and tetrahedron $\nu(SiO_4)$, respectively. The spectrum also displayed a strong band at 468 cm^{-1} which is assigned to ν(≡Si—O—Si≡) deformation [25,26]. The spectrum of amino-modified magnetic silica (MAMMS) displayed mainly the same characteristic bands of free precipitated silica with decreasing the intensity of the free silanol group at 957 cm^{-1}. Moreover, the spectrum of MAMMS is characterized by the appearance of two weak bands near 2860 and 2937 cm^{-1} that are assigned to $\nu(CH_2)$ stretching. The above behavior gives a good clue for the success of the modification process. The spectrum of the silica-coated magnetite was also characterized by the appearance of (Fe–OH) vibrations in 561–638 cm^{-1} range [27]. The presence of magnetite in the precipitated silica was also confirmed from XRD measurements. As shown in Fig. 3, Fe_3O_4 displayed a number of diffraction lines at 2θ (18.22, 30.28, 35.41, 43.25, 57.26 and 62.84). These lines are characteristic for spinel Fe_3O_4. The pattern of silica-coated magnetite displayed the same lines, especially the most intense one at 2θ (35.41) confirming the presence of magnetite. As shown in Table 1, the magnetite containing silica (MAMMS) shows a lower values for surface area (BET) as well as pore volume relative to those of magnetite free one (MAMPS). This may be attributed to the presence of embedded magnetite particles as shown in Fig. 1.

Table 1
Textural properties of the studied silicas.

Property	MAMPS	MAMMS
BET surface area ($m^2\ g^{-1}$)	79.40	52.09
Pore volume ($cm^3\ g^{-1}$)	3.08×10^{-2}	2.33×10^{-2}
Pore diameter (Å)	0.155	0.179

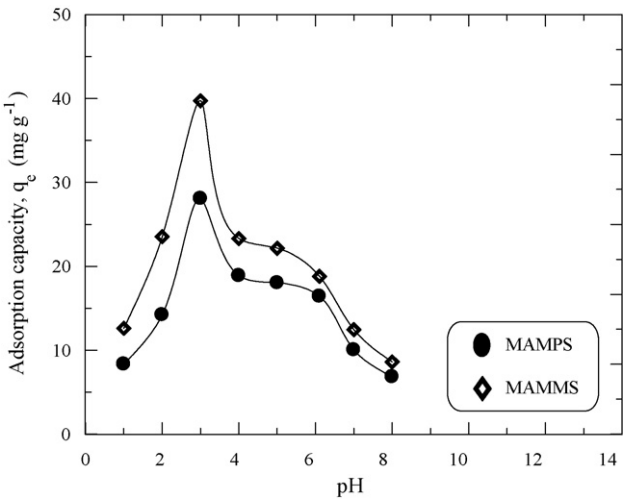

Fig. 4. Effect of pH on the adsorption of AO-10 on MAMPS and MAMMS at 298 K.

5.2. Adsorption studies

5.2.1. Effect of pH

The effect of pH on the adsorption of AO-10 dye on modified silica at 298 K is shown in Fig. 4. The maximum adsorption was observed at pH 3 for both silica samples. The adsorption of AO-10 dye may be explained to proceed via the electrostatic attraction between the positively charged protonated amino groups on the silica surface ($-NH_3^+$) and the negatively charged sulfonate groups (SO_3^-) of the dye [28,29]:

$$\text{Silica-NH}_2 + \text{HCl} \rightarrow \text{Silica-NH}_3^+\text{Cl}^-$$

$$\text{Silica-NH}_3^+\text{Cl}^- + \text{D-SO}_3^-\text{Na}^+ \rightarrow \text{Silica-NH}_3^+{}^-\text{O}_3\text{S-D} + \text{NaCl}$$

The observed higher adsorption capacity of AO-10 on MAMMS relative to MAMPS may be attributed to the formation of thin film of silica on the magnetite particles that increases the number of exposed active sites available for interaction with the dye as shown in Fig. 1. The decrease in the adsorption capacity of the dye at pH < 3 could be attributed to the decrease in the dissociation of the dye which leads to a lower concentration of the anionic species to interact with the active sites of silica [30]. It is also seen that the adsorption decreases as the pH of medium increases. This may be attributed to the deprotonation of amino groups along with the formation of negatively charged silanolate groups (≡SiO^-) that repel the sulfonate groups (SO_3^-) of the dye from interaction with the surface. The optimized structure of the dye and its interaction with the surface are shown in Fig. 5. Inspection of Fig. 5 indicates that minimum energy structure of AO-10 (with respect to modified silica surface) adopts a twisted configuration [31].

5.2.2. Isotherms

The results of the effect of the temperature on the adsorption capacity of the dye on both silica samples are shown in Fig. 6. Obviously, the adsorption capacity decreases as the temperature increases in both cases. This implies that AO-10 adsorbs physically on the surface of two silica samples. Fig. 7 shows the change of the adsorption capacity of both silica samples as a function of initial concentration of the dye. Inspection of Fig. 7 reveals that the adsorption capacity of the dye on MAMMS is higher than that on MAMPS at all concentration ranges. The maximum adsorption capacities at 298 K are 48.98 and 61.33 mg g^{-1} for MAMPS and MAMMS, respectively. The higher adsorption capacity in the case of MAMMS may be attributed to the formation of thin film of silica on magnetite fine particles that facilitates the interaction between dye species with

Table 2
Isotherm constants for the adsorption of AO-10 on modified silicas at 298 K.

Adsorbent	q_{exp} (mg g^{-1})	Non-linear Langmuir isotherm model					Non-linear Freundlich isotherm model			
		Q_{max} (mg g^{-1})	K_L (dm^3 mg^{-1})	S.E.	R_L	R^2	$1/n$	K_F (dm^3 mg^{-1})	S.E.	R^2
MAMPS	48.98	65.89	0.087	0.002	0.044	0.9962	0.19	24.89	1.536	0.9552
MAMMS	61.33	61.14	0.245	0.003	0.020	0.9994	0.17	28.35	0.465	0.9876

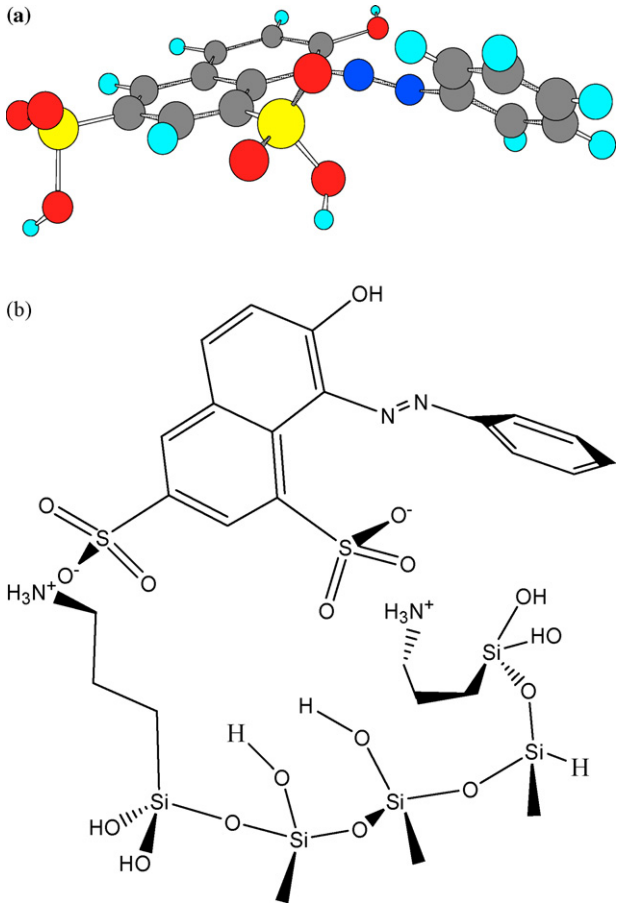

Fig. 5. Chemical structure of AO-10 (a) and the mechanism of interaction between the modified silica and AO-10 (b).

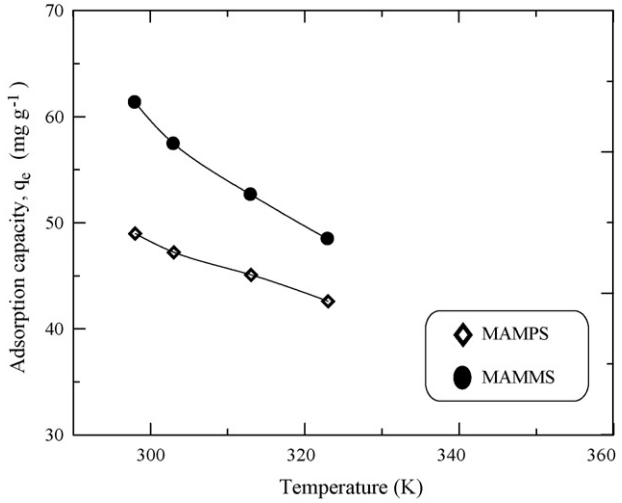

Fig. 6. Effect of temperature on the adsorption of AO-10 on MAMPS and MAMMS.

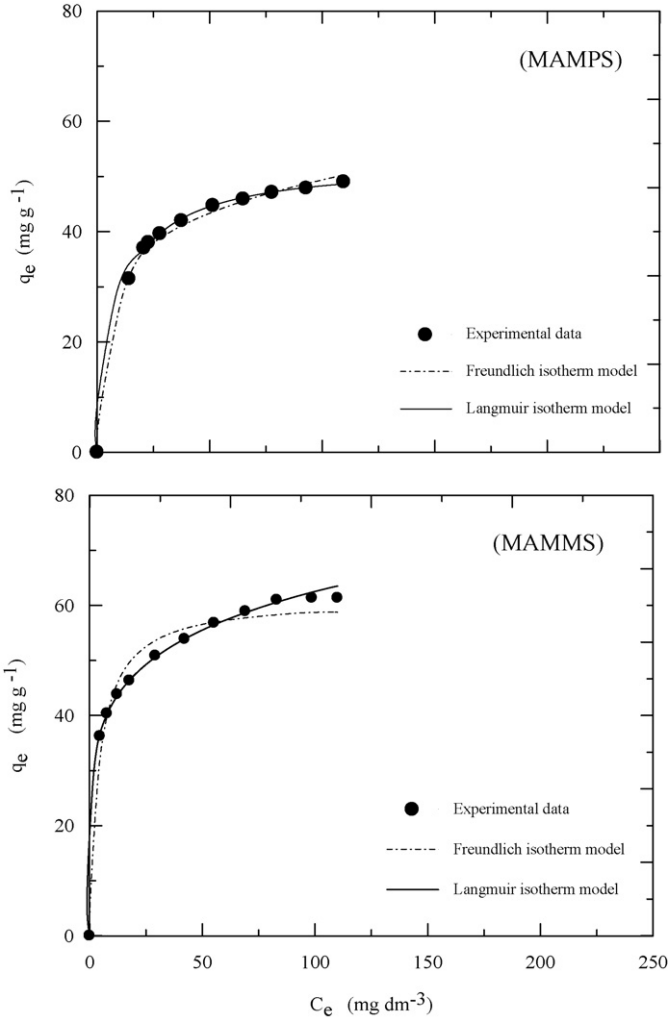

Fig. 7. Isotherms of adsorption of AO-10 on MAMPS and MAMMS at 298 K.

silica active sites. The lower adsorption capacity of MAMPS in spite of its higher surface area and pore volume compared to MAMMS (Table 1) may be attributed to the inaccessibility of the dye ions for intraparticle diffusion in the case of MAMPS to be adsorbed on the internal surface of silica. The adsorption data of Fig. 7 were treated according to Langmuir and Freundlich models [1]:

$$q_e = \frac{Q_{max} K_L C_e}{1 + K_L C_e} \quad (2)$$

$$q_e = K_F C_e^{1/n} \quad (3)$$

where C_e is the equilibrium concentration of dyes with (mg dm^{-3}), q_e is the adsorption capacity at equilibrium state (mg g^{-1}), Q_{max} is the theoretical maximum adsorption capacity (mg g^{-1}), K_L is the Langmuir isotherm constant which is related to the strength of adsorbent/adsorbate interaction (dm^3 mg^{-1}), K_F and n are the Freundlich constants related to the adsorption capacity and intensity, respectively. The experimental data were fitted to the above models

Table 3
Langmuir parameters for MAMPS and MAMMS at different temperatures.

Temperature (K)	MAMPS			MAMMS		
	Q_{max} (mmol g^{-1})	$K_L \times 10^3$ (dm^3 mol^{-1})	R^2	Q_{max} (mmol g^{-1})	$K_L \times 10^3$ (dm^3 mol^{-1})	R^2
298	0.117	49.09	0.9962	0.135	110.83	0.9876
313	0.116	29.04	0.9977	0.133	54.69	0.9955
323	0.114	25.38	0.9958	0.126	36.14	0.9985
333	0.112	21.08	0.9958	0.125	22.20	0.9979

Table 4
Thermodynamic parameters of adsorption of AO-10 on MAMPS and MAMMS.

Temperature (K)	MAMPS				MAMMS			
	ΔG^0 (kJ mol^{-1})	$T\Delta S^0$ (kJ mol^{-1})	ΔH^0 (kJ mol^{-1})	ΔS^0 (J mol^{-1} K^{-1})	ΔG^0 (kJ mol^{-1})	$T\Delta S^0$ (kJ mol^{-1})	ΔH^0 (kJ mol^{-1})	ΔS^0 (J mol^{-1} K^{-1})
298	−26.52	7.91	−18.60	26.56	−28.49	−4.74	−33.23	−15.91
313	−26.91	8.31			−28.25	−4.98		
323	−27.18	8.58			−28.09	−5.14		
333	−27.44	8.84			−27.93	−5.30		

using SPSS software (version 10). The values of the Langmuir and Freundlich constants were calculated from the nonlinear regression for each model at 298 K and are reported in Table 2. From Fig. 7, the experimental data of adsorption of the dye on MAMPS and MAMMS are better fit to Langmuir model than Freundlich model. The values of R^2 and standard error (S.E.), which are a measure of the goodness-of-fit, confirm the good representation of the experimental data by Langmuir model. This indicates the homogeneity of active sites on the surface of MAMPS and MAMMS with higher extent in the case of the latter. The values of K_L are given in Table 3 for MAMPS and MAMMS at different temperatures. The difference in the values of K_L for MAMPS and MAMMS refers the different binding strength of the dye with amine groups on the surface of both silicas.

The essential features of Langmuir adsorption isotherm can be expressed in terms of a dimensionless constant called separation factor or equilibrium parameter (R_L), which is defined by the following relationship [32]:

$$R_L = \frac{1}{1 + K_L C_0} \quad (4)$$

where C_0 is the initial concentration of dye (mg dm^{-3}). The value of R_L indicates the nature of adsorption isotherm; irreversible ($R_L = 0$), favourable ($0 < R_L < 1$), and unfavourable ($R_L = 1$). As shown in Table 2, the calculated values of R_L were found between 0 and 1. This implies that the adsorption of the investigated dye on both modified silica samples from aqueous solutions is favourable under the conditions used in this study.

5.2.3. Thermodynamics

The thermodynamic parameters of adsorption can be derived from the following equation [33]:

$$\ln K_L = \frac{\Delta S^0}{R} - \frac{\Delta H^0}{RT} \quad (5)$$

Plotting of $\ln K_L$ against $1/T$ at different temperatures gives straight line with slope and intercept equal to $(-\Delta H^0/R)$ and $(\Delta S^0/R)$, respectively. The calculated values of ΔH^0 and ΔS^0 for the adsorption of AO-10 on silica samples are reported in Table 4. The negative values of ΔH^0 indicate that the adsorption of the dye on both modified silicas is exothermic. On the other hand, the negative values of ΔS^0 reflect the decrease of randomness of the system due to the strong binding of dye molecules on MAMMS compared to MAMPS. The data given in Table 4 show that $|\Delta H^0| > |T\Delta S^0|$ for both silica samples at all temperatures. This indicates that the adsorption process is dominated by enthalpic rather than entropic changes [34]. The Gibbs free energy (ΔG^0) of the adsorption reaction can be calculated using the following equation [34]:

$$\Delta G^0 = \Delta H^0 - T\,\Delta S^0 \quad (6)$$

The negative values of ΔG^0 reported in Table 4 indicate the spontaneity of the adsorption of the dye on modified silica used in this study.

5.3. Kinetics

Fig. 8 shows the change in the adsorption of the investigated dye on both modified silica samples as a function of time. The equilibrium was reached within 3 and 1 h for MAMPS and MAMMS, respectively. The rate of adsorption of the dye was noticed to be faster compared to that reported earlier (5 h) on modified silica of different source [31]. The adsorption/time data were treated according to two kinetics models [35]:

(i) Pseudo-first order model:

$$q_t = q_e[1 - \exp(-k_1 t)] \quad (7)$$

(ii) Pseudo-second order model:

$$q_t = \frac{ht}{1 + k_2 q_e t} \quad (8)$$

where q_e and q_t refer to the amount of dye adsorbed (mg g^{-1}) at equilibrium and at time t (min), k_1 is the overall rate constant of pseudo-first order reaction (min^{-1}), h is the initial rate constant, k_2 is the overall rate constant of the pseudo-second order reaction (g mg^{-1} min^{-1}). The experimental data were fitted to the above

Table 5
Kinetic constants for the adsorption of AO-10 on modified silicas at 298 K.

Adsorbent	MAMPS					MAMMS				
	Non-linear pseudo-first order model					Non-linear pseudo-second order model				
	$q_{e\,(exp)}$ (mg g^{-1})	$q_{e\,(calc)}$ (mg g^{-1})	k_1 (min^{-1})	S.E.	R^2	$q_{e\,(calc)}$ (mg g^{-1})	k_2 (mg g^{-1} min^{-1})	h (mg g^{-1} min^{-1})	S.E.	R^2
MAMPS	24.20	23.21	0.226	0.034	0.938	24.49	0.0182	09.63	0.002	0.9915
MAMMS	37.02	35.12	0.211	0.039	0.964	37.03	0.0102	13.94	0.001	0.9977

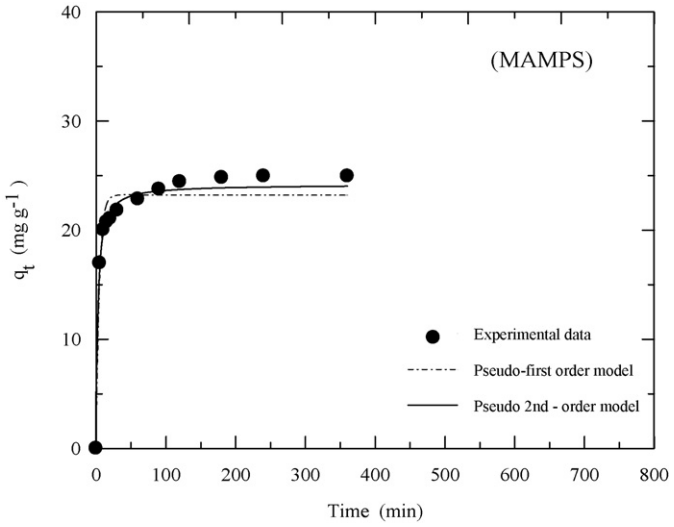

Fig. 8. Adsorption kinetics of AO-10 by MAMPS and MAMMS at 298 K.

two models using SPSS software (version 10). The kinetic parameters were calculated from the nonlinear regression for each model and are given in Table 5. The experimental data were found to fit the pseudo-second order model where a satisfactory agreement was obtained between the calculated and the experimental values of q_e. The values of the initial rate constant (h) for MAMMS are greater than that of MAMPS. This indicates the higher rate of adsorption of the dye on MAMMS as a consequence of the increase of the efficient interaction between the dye ions and the silica active sites.

5.4. Desorption

Desorption of the loaded dye was carried out at pH 7–10 and the data are reported in Table 6. The elution of the dye from modified silica surface may be explained on the basis of deprotonation of the amine groups under basic conditions. Thus the electrostatic interaction with the dye anions would decrease dramatically as follows:

$$\text{Silica-NH}_3{}^+{}^-\text{O}_3\text{S-D} + \text{NaOH} \rightarrow \text{Silica-NH}_2 + \text{D-SO}_3\text{Na} + \text{H}_2\text{O}$$

Over three adsorption/desorption cycles, the elution efficiency was found to be 98.1% and 98.8 ± 1% for MAMPS and MAMMS at pH 10, respectively.

6. Conclusions

Amine-modified magnetic silica samples were obtained through precipitation of sodium silicate using HCl in absence and presence of suspended magnetite fine particles. The silica-containing magnetite (MAMMS) showed higher adsorption capacity towards the acidic dye AO-10 relative to magnetite-free silica (MAMPS). The maximum adsorption was recorded at pH 3 for both silica samples. Thermodynamic studies revealed the spontaneity of the adsorption that became unfavourable at higher temperature. Kinetics studies revealed that adsorption of AO-10 on MAMMS was fast compared to MAMPS due to the less porous structure of the former. Regeneration of the adsorbents was easy done using NaOH at pH 10 reaching efficiency of 98%.

Table 6
Desorption ratio of dye-loaded MAMS at different pHs.

pH	Desorption ratio (%)	
	MAMPS	MAMMS
7	20.6	30.5
8	40.4	60.5
9	70.3	80.7
10	98.1	98.8

References

[1] F.A. Batzias, D.K. Sidiras, Simulation of dye adsorption by beech sawdust as affected by pH, J. Hazard. Mater. B141 (2007) 668–679.
[2] M. Muthukumar, M.T. Karuppiah, G.B. Raju, Electrochemical removal of C.I. acid orange 10 from aqueous solutions, Sep. Purif. Technol. 55 (2007) 198–205.
[3] A.R. Cestari, E.F.S. Vieira, A.A. Pinto, E.C.N. Lopes, Multistep adsorption of anionic dyes on silica/chitosan hybrid. 1. Comparative kinetic data from liquid- and solid-phase models, J. Colloid Interface Sci. 292 (2005) 363–372.
[4] Y.C. Wong, Y.S. Szeto, W.H. Cheung, G. Mckay, Pseudo-first-order kinetic studies of the sorption of acid dyes onto chitosan, J. Appl. Polym. Sci. 92 (2004) 1633–1645.
[5] P. Baskaralingam, M. Pulikesi, D. Elango, V. Ramamurthi, S. Sivanesan, Adsorption of acid dye onto organobentonite, J. Hazard. Mater. B128 (2006) 138–144.
[6] S.J. Allen, B. Koumanova, Decolourisation of water/wastewater using adsorption (review), J. Chem. Technol. Metal. 40 (2005) 175–192.
[7] P. Baskaralingam, M. Pulikesi, D. Elango, V. Ramamurthi, S. Sivanesan, Equilibrium studies for the adsorption of acid dye onto modified hectorite, J. Hazard. Mater. B 136 (2006) 989–992.
[8] G. Crini, Non-conventional low-cost adsorbents for dye removal: a review, Bioresour. Technol. 97 (2006) 1061–1085.
[9] S.J. Allen, G. Mckay, J.F. Porter, Adsorption isotherm models for basic dye adsorption by peat in single and binary component systems, J. Colloid Interface Sci. 280 (2004) 322–333.
[10] W.T. Tsai, C.Y. Chang, C.H. Ing, C.F. Chang, Adsorption of acid dyes from aqueous solution on activated bleaching earth, J. Colloid Interface Sci. 275 (2004) 72–78.
[11] Z.G. Hu, J. Zhang, W.L. Chan, Y.S. Szeto, The sorption of acid dye onto chitosan nanoparticles, Polymer 47 (2006) 5838–5842.
[12] Z. Bouberka, A. Khenifi, N. Benderdouche, Z. Derriche, Removal of Supranol Yellow 4 GL by adsorption onto Cr-intercalated montmorillonite, J. Hazard. Mater. B 133 (2006) 154–161.
[13] P.V. Messina, P.C. Schulz, Adsorption of reactive dyes on titania–silica mesoporous materials, J. Colloid Interface Sci. 299 (2006) 305–320.
[14] A.R. Cestari, E.F.S. Vieira, E.S. Silva, Interactions of anionic dyes with silica–aminopropyl. 1. A quantitative multivariate analysis of equilibrium adsorption and adsorption Gibbs free energies, J. Colloid Interface Sci. 297 (2006) 22–23.
[15] X. Liu, Z. Ma, J. Xing, H. Liu, Preparation and characterization of amino–silane modified superparamagnetic silica nanospheres, J. Magn. Magn. Mater. 270 (2004) 1–6.
[16] M.E. Park, J.H. Chang, High throughput human DNA purification with aminosilanes tailored silica-coated magnetic nanoparticles, Mater. Sci. Eng. C27 (2007) 1232–1235.
[17] A.D. Campo, T. Sen, J.P. Lellouche, I.J. Bruce, Multifunctional magnetite and silica–magnetite nanoparticles: synthesis, surface activation and applications in life sciences, J. Magn. Magn. Mater. 293 (2005) 33–40.
[18] Z. Ma, Y. Guan, H. Liu, Superparamagnetic silica nanoparticles with immobilized metal affinity ligands for protein adsorption, J. Magn. Magn. Mater. 301 (2006) 469–477.
[19] A.E. David, N.S. Wang, V.C. Yang, A.J. Yang, Chemically surface modified gel (CSMG): an excellent enzyme-immobilization matrix for industrial processes, J. Biotechnol. 125 (2006) 395–407.
[20] M. Dakiky, A. Manassra, M. Abdul Kareem, F. Jumean, M. Khamis, Acid alizarin violet interactions with surfactants: ionization and thermodynamic parameters in buffered cationic, anionic and nonionin surfactant solutions, Dyes Pigments 63 (2004) 101–113.
[21] Y. Sun, M. Ma, Y. Zhang, N. Gu, Synthesis of nanometer-size maghemite particles from magnetite, Colloids Surf. A: Physicochem. Eng. Asp. 245 (2004) 15–19.
[22] F. Peditto, Ph.D. thesis in material science and technology, 2004. <http://docinsa.insa-lyon.fr/these/pont.php?id=peditto>.
[23] M.J.S. Dewar, AM1: a new general purpose quantum mechanical molecular model, J. Am. Chem. Soc. 107 (1985) 3902–3909.
[24] M.J. Frisch, et al., Gaussian 98W, Revision A. 7, Gaussian Inc., Pittsburgh, PA, USA, 1998.
[25] J. Lin, J.A. Siddiqui, R.M. Ottenbrite, Surface modification of inorganic oxide particles with silane coupling agent and organic dyes, Polym. Adv. Technol. 12 (2001) 285–292.
[26] J.A.A. Sales, C. Airoldi, Epoxide silylant agent ethylenediamine reaction product anchored on silica gel–thermodynamics of cation–nitrogen interaction at solid/liquid interface, J. Non-Cryst. Solids 330 (2003) 142–149.
[27] M. Ma, Y. Zhang, W. Yu, H. Zhang, N. Gu, Preparation and characterization of magnetite nanoparticles coated by amino silane, Colloids Surf. A: Physicochem. Eng. Asp. 212 (2003) 219–226.
[28] K. Santhy, P. Selvapathy, Removal of reactive dyes from wastewater by adsorption on coir pith activated carbon, Bioresour. Technol. 97 (2006) 1329–1336.
[29] I.D. Mall, V.C. Srivastava, N.K. Agarwal, Removal of Orange-G and Methyl Violet dyes by adsorption onto bagasse fly ash—kinetic study and equilibrium isotherm analyses, Dyes Pigments 69 (2006) 210–223.

[30] G. Gibbs, J.M. Tobin, E. Guibal, Sorption of Acid Green 25 on chitosan: influence of experimental parameters on uptake kinetics and sorption isotherms, J. Appl. Polym. Sci. 90 (2003) 1073–1080.
[31] A.M. Donia, A.A. Atia, W.A. Al-amrani, A.M. El-Nahas, Effect of structural properities of acid dyes on their adsorption behaviour from aqueous solutions by amine modified silica, J. Hazard. Mater. 161 (2009) 1544–1550.
[32] A. Khenifi, Z. Bouberka, F. Sekrane, M. Kameche, Adsorption study of industrial dye by an organic clay, Adsorption 13 (2007) 149–158.
[33] Y.S. Al-Degs, M.I. El-Barghouthi, A.H. El-Sheikh, G.M. Walker, Effect of solution pH, ionic strength, and temperature on adsorption behaviour of reactive dyes on activated carbon, Dyes Pigments 77 (2008) 16–23.
[34] A.M. Donia, A.A. Atia, H.A. El-Boraey, D.H. Mabrouk, Adsorption of Ag(I) on glycidyl methacrylate/N,N'-methylene bis-acrylamide chelating resins with 455 embedded iron oxide, Sep. Purif. Technol. 48 (2006) 281–287, 456.
[35] K.V. Kumar, Linear and non-linear regression analysis for the sorption kinetics of methylene blue onto activated carbon, J. Hazard. Mater. B137 (2006) 1538–1544.